

---

---

# Collimator Selection, Acquisition Speed, and Visual Assessment of $^{131}\text{I}$ -Tositumomab Biodistribution in a Phantom Model

Hung K. Tan, CNMT, Richard W. Wassenaar, PhD, and Wanzhen Zeng, MD, PhD

Division of Nuclear Medicine, Ottawa Hospital, Ottawa, Ontario, Canada

$^{131}\text{I}$ -Tositumomab has been used in treating patients with non-Hodgkin's lymphoma. It is generally recommended that high-energy collimators be used to image patients before they receive  $^{131}\text{I}$ -tositumomab therapy, to determine the effective half-life for therapeutic dose and gross biodistribution. Because many nuclear medicine departments do not possess high-energy collimators, this study was designed to assess the suitability of using medium-energy collimators. The effect of scanning speed was also investigated, in an attempt to optimize the acquisition time. **Methods:** Measurements were taken using an elliptic anthropomorphic torso phantom and an organ-scanning phantom fitted with fillable spheres (1–5 cm in diameter) and organ inserts. Three phantom studies were performed with differing initial  $^{131}\text{I}$  concentrations in the organs, the spheres, and the thoracic and abdominal chambers. Images were acquired with both high-energy and medium-energy collimators and at acquisition speeds of 20 and 100 cm/min. The half-life for each combination (study/collimator/speed) was calculated from a linear fit of the data. The contrast of the tumor sphere was assessed using 2 identical regions, placed on and beside the sphere, and averaged over several time points. Biodistribution and image quality were visually assessed by 2 independent observers. **Results:** Measured half-life values and visual assessment of biodistribution showed no significant difference between the 2 collimators ( $P = 0.32$ ) or acquisition speeds ( $P = 0.85$ ). A significant difference in the contrast of the tumor spheres was observed between the 2 collimators ( $P < 0.01$ ) but not between acquisition speeds. Visual assessment of the images showed increased noise on the image acquired at 100 cm/min, although this noise did not affect lesion detectability. **Conclusion:** Measured half-life is not significantly different between the 2 collimators; hence, calculation of the residence time would be nearly the same. Medium-energy collimators can be used to accurately calculate the  $^{131}\text{I}$ -tositumomab therapeutic dose and detect alterations in biodistribution.

**Key Words:** Bexxar; medium-energy collimators; whole-body acquisition speed

**J Nucl Med Technol 2006; 34:224–227**

**T**ositumomab labeled with  $^{131}\text{I}$  (Bexxar; GlaxoSmith-Kline Pharmaceuticals) has been used recently in treating patients with non-Hodgkin's lymphoma by targeting CD20 antigen expressed in B-lymphocytes (1–4).

A  $^{131}\text{I}$ -tositumomab therapeutic regimen consists of a dosimetric component and a therapeutic component. Whole-body counts measured at 0, 3 or 4 d and at 6 or 7 d after dosimetric  $^{131}\text{I}$ -tositumomab administration are used to determine the total-body residence time. Whole-body images are viewed to assess altered biodistribution. Organ dysfunction, such as urinary tract obstruction, can result in increased organ toxicity and poor targeting of the tumor CD20 antigen. In such a case, therapy should not be given (1).

Because of the relatively high photon energy of  $^{131}\text{I}$  (364 keV), it is recommended that a high-energy, parallel-hole collimator be used for the dosimetric study. However, many nuclear medicine departments, particularly smaller departments, do not have a set of high-energy collimators. Such being the case, it is important to assess the suitability of using medium-energy collimators for the dosimetric study. Compared with high-energy collimators, medium-energy collimators offer increased detection efficiency. However, scatter is also increased because of the higher septal penetration.

In this study, the application of medium-energy collimators in measuring  $^{131}\text{I}$ -tositumomab biodistribution, half-life, and lesion detectability was assessed both visually and quantitatively using an anthropomorphic phantom model. The results were compared with results obtained using high-energy collimators. As well, the effect of image acquisition speed was assessed for both the high-energy and the medium-energy collimators. It is important to optimize this parameter to decrease imaging time and increase throughput while maintaining image quality.

## MATERIALS AND METHODS

An elliptic anthropomorphic torso phantom (Data Spectrum) with lung, liver, and heart inserts was used with an organ-scanning phantom (The Phantom Laboratory) containing liver, spleen, and kidney inserts as the model.

Because of the use of 2 phantoms, the distance between the heart/lungs and abdominal organs was increased, as seen by the

---

Received Jun. 13, 2006; revision accepted Sep. 11, 2006.  
For correspondence or reprints contact: Wanzhen Zeng, MD, PhD, Division of Nuclear Medicine, Ottawa Hospital, Civic Campus, 1053 Carling Ave., Ottawa ON, Canada, K1Y 4E9.  
E-mail: wzeng@ottawahospital.on.ca  
COPYRIGHT © 2006 by the Society of Nuclear Medicine, Inc.

increased area of background counts between the heart/lungs and abdominal organs (Fig. 1). A set of hollow spheres with diameters of 1–5 cm was placed in the abdominal cavity to simulate tumor lesions.

All studies were acquired on a dual-head  $\gamma$ -camera (e.cam; Siemens) with a 15% symmetric energy window centered on the 364-keV photopeak of  $^{131}\text{I}$ . The camera heads were positioned directly beneath and 30 cm above the imaging table to acquire the posterior and anterior views, respectively.

### Study Protocols

Clinically, 3 whole-body images are acquired on different days to assess  $^{131}\text{I}$ -tositumomab biologic decay and biodistribution. To simulate the varying biodistribution resulting from biologic and physical decay, 3 experiments were performed with various radiotracer concentrations in the organs and spheres. Phantom activity was estimated on the basis of the relative whole-body counts measured at different time points by Dr. Seldin et al. (5). The percentage of activity in each organ was based on the measured activity of approximately 100 patients collected by Corixa (Haren D. Rupani, written communication, January 2005).

*Experiment 1.* The concentration of  $^{131}\text{I}$  in the organs was similar to that of a patient's biodistribution on the same day as  $^{131}\text{I}$ -tositumomab administration (Table 1). Whole-body phantom images were acquired for 5 time points (0, 2, 4, 8, and 13 d after  $^{131}\text{I}$  administration) for both the high-energy and the medium-energy collimators. At each time point, images were acquired using speeds of 20 and 100 cm/min. Three tumor spheres (diameters of 3, 4, and 5 cm) of 18 MBq/L concentration were placed in the abdominal chamber. The whole-body activity was 74 MBq.

*Experiment 2.* The concentration of  $^{131}\text{I}$  in the organs and tumor spheres was similar to that of a patient's biodistribution on day 3 after  $^{131}\text{I}$  administration (Table 1). Acquisition and measurements similar to those of experiment 1 were performed on days 0, 2, 5, 9, and 12. The whole-body activity was 92 MBq.

*Experiment 3.* This experiment was designed to test the ability of the medium-energy collimators to detect low-contrast lesions of various sizes. The concentration of  $^{131}\text{I}$  activity in the organs was identical to that used in experiment 1 (Table 1). In addition, 6 tumor spheres (diameters of 1, 1.5, 2, 3, 4, and 5 cm) of 740 MBq/L concentration were placed within the abdominal cavity. Images were acquired on 0, 2, 5, and 9 d after  $^{131}\text{I}$  administration at acquisition speeds of 20 and 100 cm/min.

Before each experiment, 1-min background images were acquired with both the high-energy and the medium-energy collimators. These images were used to correct the whole-body activity for background activity.

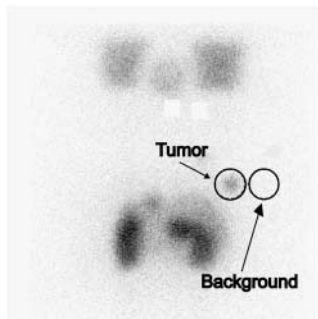


**FIGURE 1.** Total counts from identical circular regions placed over the 4-cm sphere and over an area of background were used to determine tumor-to-background contrast.

Collimator sensitivity was measured using a standard  $^{131}\text{I}$  point source of approximately 7.4 MBq in 2 mL of water, contained in a 3-mL syringe. The source was imaged at each time point using the camera head positions defined above, and the activity was measured using a dose calibrator.

### Data Analysis

For each experiment, the total whole-body counts, corrected for background activity, were plotted as a function of time on a semi-log plot. The half-life was calculated from a linear least-squares fit of the data, along with the 95% confidence interval. This 95% confidence interval was used to determine half-life agreement between collimators. Three-way ANOVA was performed to study the intercollimator, interexperiment, and interspeed variations in half-life measurements.

The  $\gamma$ -camera sensitivity was defined as the ratio of the total counts from the  $^{131}\text{I}$  point source images divided by the activity measured in the dose calibrator. Mean sensitivity (over all time points and experiments) and the coefficient of variation were calculated for both the high-energy and the medium-energy collimators.

Tumor-to-background contrast was measured using 2 identical, circular regions of interest placed over and beside the 4-cm sphere on the posterior image, as shown in Figure 1. The contrast was calculated as the ratio of counts in the region of interest over the sphere to counts in the region of interest over the background. This ratio was calculated for both the high-energy and the medium-energy collimators and at speeds of 20 and 100 cm/min. The mean contrast (averaged over the time points) and 1 SD are reported. A paired *t* test was used to compare the contrast between acquisition speeds and collimators.

All images (acquired at the various time points, acquisition speeds, etc.) were visually assessed by a nuclear medicine physician and nuclear medicine physicist working independently. Each observer adjusted the color intensity before assessing the images. The observers noted overall image quality, whether all tumor spheres could be identified on the image, and whether the relative organ tracer distributions were altered from the normal biodistribution. The observers were aware of collimator selection and acquisition speed, which were apparent based on image quality. Background activity was increased on images acquired using the fast speed or the medium-energy collimators.

## RESULTS

### Half-Life Measurement

The calculated half-life values of the anterior whole-body decay curves, along with the 95% confidence interval, are presented in Table 2. Three-way ANOVA indicated no difference in half-life values between collimators ( $P = 0.32$ ) or acquisition speeds ( $P = 0.85$ ) but a significant difference between experiments ( $P < 0.001$ ).

The sensitivity of the  $\gamma$ -camera was found to be 2.3 and 6.5 kcts/MBq for the high-energy and medium-energy collimators, respectively. The coefficient of variation of the sensitivities was calculated to be 2.0% and 2.5% with the high-energy and medium-energy collimators, respectively.

### Visual Assessment

Visual assessment of all the images indicated no differences between the high-energy and medium-energy

**TABLE 1**  
<sup>131</sup>I Organ Concentrations (MBq/L) Used in Each Experiment (5)

Experiment	Kidneys	Lungs	Liver	Spleen	Heart	Background	Sphere
1	51.1	38.5	40.3	76.2	118	0.148	185
2	41.1	23.3	23.3	49.2	8.88	0.148	144
3	51.1	38.5	40.3	76.2	118	0.148	74

collimators in terms of organ tracer distribution. However, background activity was increased on the images acquired with medium-energy collimators, likely because of increased scattering. Image quality was visually superior at an acquisition speed of 20 cm/min than at 100 cm/min, because of the increase in counts at 20 cm/min. Tumor detectability was unaffected by acquisition speed: All tumor spheres were visualized, regardless of acquisition speed.

In experiments 1 and 2, with the tumor sphere concentration approximately twice that in the spleen, the 2 tumor lesions in the right and left upper quadrants were visualized on all images, as shown in Figure 2. Another tumor sphere, embedded between the liver and spleen, was only faintly visualized on all images. In experiment 3, with the lower <sup>131</sup>I concentration in the spheres, the 2-cm tumor sphere in the right upper abdomen was clearly visualized on images acquired with high-energy collimators but poorly visualized on images acquired with medium-energy collimators.

#### Tumor Contrast

Tumor-to-background contrast, presented in Table 2, was significantly lower with medium-energy collimators ( $P < 0.01$ ) for all experiments and at both speeds. However, acquisition speed did not affect contrast ( $P =$  not statistically significant).

#### DISCUSSION

The current therapeutic regimen is based on several factors, including the patient's weight or body surface area, bone marrow dosimetry, and the residence time of <sup>131</sup>I-tositumomab. Residence time is calculated by sequential measurement of whole-body counts. This study found

that the half-life value measured from the sequential whole-body images did not change with medium-energy collimators. As well, the use of medium-energy collimators did not alter the gross biodistribution of tracer uptake by individual organs, as assessed by 2 independent observers. This finding indicates that the use of medium-energy collimators is suitable for assessment of <sup>131</sup>I-tositumomab residence time.

The current recommended scanning speed of 10–30 cm/min results in a maximum scanning time of 20 min for a whole-body scan. In the <sup>131</sup>I-tositumomab study protocol, 3 whole-body scans are required before the final treatment, for a total scanning time of approximately 1 h. This length of time can place a significant burden on a busy nuclear medicine department. This study demonstrated that a scanning speed of 10–30 cm/min may be conservative. Half-life values and tumor-to-background contrast were not significantly different when a 100 cm/min acquisition speed was used. However, a noticeable increase in noise was associated with the lower counts but, again, did not adversely affect half-life values.

With the use of medium-energy collimators, a decrease in tumor-to-background contrast was found, along with a decrease in the visualization of small tumors. This observation may have a significant application in tumor response assessment. Tumor response, assessed by the tumor counts after therapy, has been shown to be related to tumor radiation dose (4). Our study demonstrated that the counts-to-activity conversion factor is dependent on the level of background activity and the collimator selection. The use of medium-energy collimators may decrease the accuracy of assessing quantitative tumor response and should be used with caution.

**TABLE 2**  
Half-Life ( $t_{1/2}$ ) with 95% Confidence Interval (CI) and Tumor-to-Background Contrast Ratios for All Experiments Using Both High-Energy and Medium-Energy Collimators

Acquisition speed (cm/min)	Collimator type	Experiment 1			Experiment 2			Experiment 3		
		$t_{1/2}$ (d)	95% CI (d)	Contrast $\pm 1\sigma$	$t_{1/2}$ (d)	95% CI (d)	Contrast $\pm 1\sigma$	$t_{1/2}$ (d)	95% CI (d)	Contrast $\pm 1\sigma$
20	High-energy	8.3	8.1, 8.6	6.6 $\pm$ 0.7	7.9	7.6, 8.2	7.5 $\pm$ 0.7	8.4	7.8, 9.2	3.9 $\pm$ 0.5
	Medium-energy	8.5	8.2, 8.7	2.5 $\pm$ 0.1*	7.8	7.5, 8.1	3.0 $\pm$ 0.1*	8.6	8.0, 9.2	2.4 $\pm$ 0.3*
100	High-energy	8.4	8.0, 8.8	6.6 $\pm$ 0.3	8.0	7.7, 8.4	6.8 $\pm$ 0.4	8.4	7.6, 9.2	4.0 $\pm$ 0.5
	Medium-energy	8.5	8.2, 8.8	2.6 $\pm$ 0.2*	7.9	7.6, 8.1	3.0 $\pm$ 0.1*	8.5	8.0, 9.0	2.3 $\pm$ 0.2*

\* $P < 0.01$ , compared with high-energy collimators at same speed.

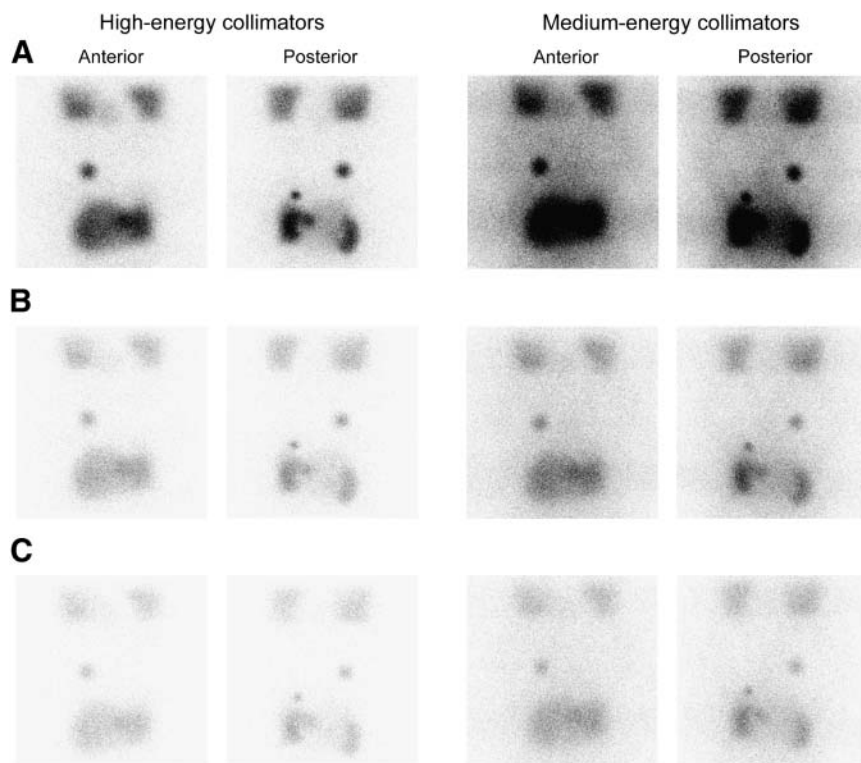


**FIGURE 2.** Anterior and posterior images using high- and medium-energy collimators for acquisition speeds of 20 (A), 60 (B), and 100 (C) cm/min. All images have been adjusted to the same color scale to better illustrate differences in image quality.

Nevertheless, the decreased visualization of small tumors with medium-energy collimators would not affect  $^{131}\text{I}$ -tositumomab treatment, because the purpose of the scans is to detect gross alterations in biodistribution rather than to reveal tumor sites. Studies have shown that the whole-body tumor burden has no impact on the overall response to, or toxicity of,  $^{131}\text{I}$ -tositumomab therapy (6,7). Furthermore, all patients should be treated, regardless of whether tumors are visualized in the dosimetric study, because the purpose of the scans is solely to detect alterations in biodistribution (8–11).

## CONCLUSION

The measured  $^{131}\text{I}$ -tositumomab half-life and organ activity were not affected by the collimator selection. Medium-energy collimators can be used to assess  $^{131}\text{I}$ -tositumomab therapeutic dose and to detect alterations in biodistribution. A faster acquisition speed can be used without compromising calculations of residence time or detection of altered biodistribution.

## ACKNOWLEDGMENTS

This work was supported by a grant from GlaxoSmith-Kline Pharmaceuticals. The authors thank Dr. Rupani for

helpful suggestions and for providing  $^{131}\text{I}$ -tositumomab biodistribution data of lymphoma patients.

## REFERENCES

1. Juweid ME. Radioimmunotherapy of B-cell non-Hodgkin's lymphoma: from clinical trials to clinical practice. *J Nucl Med.* 2002;43:1507–1529.
2. Vose JM, Wahl RL, Saleh M, et al. Multicenter phase II study of iodine-131 tositumomab for chemotherapy-relapsed/refractory low-grade and transformed low-grade B-cell non-Hodgkin's lymphomas. *J Clin Oncol.* 2000;18:1316–1323.
3. Kaminski MS, Zelenetz AD, Press OW, et al. Pivotal study of iodine I 131 tositumomab for chemotherapy-refractory low-grade or transformed low-grade B-cell non-Hodgkin's lymphomas. *J Clin Oncol.* 2001;19:3918–3921.
4. Koral KF, Dewaraja Y, Li J, et al. Update on hybrid conjugate-view SPECT tumor dosimetry and response in  $^{131}\text{I}$ -tositumomab therapy of previously untreated lymphoma patients. *J Nucl Med.* 2003;44:457–464.
5. Seldin DW. Techniques for using Bexxar for the treatment of non-Hodgkin's lymphoma. *J Nucl Med Technol.* 2002;30:109–114.
6. Sharkey RM, Brenner A, Burton J, et al. Radioimmunotherapy of non-Hodgkin's lymphoma with  $^{90}\text{Y}$ -DOTA humanized anti-CD22 IgG ( $^{90}\text{Y}$ -epratuzumab): do tumor targeting and dosimetry predict therapeutic response? *J Nucl Med.* 2003;44:2000–2018.
7. Sgouros G, Squeri S, Ballangrud AM, et al. Patient-specific, 3-dimensional dosimetry in non-Hodgkin's lymphoma patients treated with  $^{131}\text{I}$ -anti-B1 antibody: assessment of tumor dose-response. *J Nucl Med.* 2003;44:260–268.
8. Goldenberg DM, Sharkey RM. Radioimmunotherapy of non-Hodgkin's lymphoma revisited. *J Nucl Med.* 2005;46:383–384.
9. Postema EJ. Dosimetry and radioimmunotherapy of non-Hodgkin's lymphoma [letter]. *J Nucl Med.* 2004;45:2126–2127.
10. Rajendran JG, Fisher DR, Gopal AK, Durack LD, Press OW, Eary JF. High-dose  $^{131}\text{I}$ -tositumomab (anti-CD20) radioimmunotherapy for non-Hodgkin's lymphoma: adjusting radiation absorbed dose to actual organ volumes. *J Nucl Med.* 2004;45:1059–1064.
11. Britton KE. Radioimmunotherapy of non-Hodgkin's lymphoma. *J Nucl Med.* 2004;45:924–925.